Adsorption of Cadmium on Anatase Nanoparticles—Effect of Crystal Size and pH

Y. Gao,† R. Wahi,‡ A. T. Kan,*,† J. C. Falkner,‡ V. L. Colvin,‡ and M. B. Tomson†

Department of Civil and Environmental Engineering, Energy, MS-519, and Chemistry Department, MS-60, Center for Biological and Environmental Nanotechnology, Rice University, Houston, Texas 77005-1892

Received March 15, 2004. In Final Form: August 12, 2004

The adsorption and desorption of Cd^{2+} to large and nanometer-scale anatase crystals have been studied to determine the relationship between heavy metal adsorption properties and anatase particle size. A solvothermal method was used to synthesize very fine anatase nanocrystals with average grain sizes ranging from 8 to 20 nm. On a surface area basis, it was found that large and nanometer-scale anatase particles had similar maximum Cd^{2+} adsorption capacities, while their adsorption slopes differed by more than 1 order of magnitude. The particle-size effect on adsorption is constant over a pH range of 4−7.5. The desorption of Cd^{2+} from both particle sizes is completely reversible. The adsorption data have been modeled by the Basic Stern model using three monodentate surface complexes. It is proposed that intraparticle electrostatic repulsion may reduce the adsorption free energy significantly for nanometer-sized particles.

Introduction

Anatase is a widely used industrial material with a variety of applications, including pigments, cosmetics, ceramics, solar cells, and photocatalytic reactions. A number of synthetic processes, for example, aerosol pyrolysis,[1−6] sol−gel methods,[7−9] and hydrothermal and solvothermal processes,[10−15] have been developed to prepare nanocrystalline anatase. Nanometer-scale materials possibly exhibit different physical, chemical, and biological properties that may not be predictable from observations on larger-sized materials. It has been observed that the various forms of anatase exhibit different surface structural arrangements with different surface catalytic reactivity.[16−20] For example, Martra[21] reported that large anatase and nanometer-scale TiO_2 exhibit different dominant surface planes leading to very different chemical behavior, surface acidity, and catalytic reactivity. Yet little is known about the relationship between adsorptive properties of anatase and particle size.

To aid in the investigation of the size dependence of adsorption behavior, the authors' research groups have developed a solvothermal method for synthesizing very fine anatase nanocrystals with average grain sizes ranging from 8 to 20 nm. This method involves hydrolysis of a metal alkoxide precursor in the parent alcohol so as to prevent the formation of counterions in the reaction medium, thus, ensuring a relatively clean product. Preliminary models of the nanocrystal growth process in this system have allowed for some tuning of nanoparticle size, primarily through variations in temperature. However, more thorough studies of the dependence of growth on this and other reaction parameters are still needed to achieve very fine size control.

In environmental applications, nanocrystalline anatase has been used as a powerful photocatalyst to degrade both organic and inorganic pollutants in remediation and wastewater treatments.[22,23] On the other hand, the accidental release of anatase into aquatic systems is inevitable as more and more industrial applications are found for this nanomaterial. The potential environmental impact of nanometer scale anatase is largely unknown. Bulk anatase is environmentally benign, and, therefore, the environmental risks of nanometer-scale anatase may also be very small. However, it is possible that the combination of small size, high surface area, and reactivity could render nanometer scale anatase, and nanomaterials in general, more environmentally hazardous than large crystalline materials. Depending on their mobility, nanoparticles could have a significant impact on the fate of

* Corresponding author. Tel.: 713-348-5224. Fax: 713-348-5203. E-mail: atk@rice.edu.

† Department of Civil and Environmental Engineering, Energy, Rice University.

‡ Chemistry Department, Rice University.

(1) Ahonen, P. P.; Kauppinen, E. I.; Joubert, J. C.; Deschanvres, J. L.; Van Tendeloo, G. *J. Mater. Res.* **1999**, *14*, 3938−3948.

(2) Depero, L. E.; Marino, A.; Allieri, B.; Bontempi, E.; Sangaletti, L.; Casale, C.; Notaro, M. *J. Mater. Res.* **2000**, *15*, 2080−2085.

(3) Li, Y.; Ishigaki, T. *Chem. Mater.* **2001**, *13*, 1577−1584.

(4) Li, Y.; Ishigaki, T. *J. Cryst. Growth* **2002**, *242*, 511−516.

(5) Oh, S.-M.; Park, D.-W. *Thin Solid Films* **2001**, *386*, 233−238.

(6) Rulison, A. J.; Miquel, P. F.; Katz, J. L. *J. Mater. Res.* **1996**, *11*, 3083−3089.

(7) Arnal, P.; Corriu, R. J. P.; Leclercq, D.; Mutin, P. H.; Vioux, A. *J. Mater. Chem.* **1996**, *6*, 1925−1932.

(8) Ding, X.-Z.; Liu, X.-H. *Mater. Sci. Eng., A* **1997**, *224*, 210−215.

(9) Ding, X.-Z.; Qi, Z.-Z.; He, Y.-Z. *J. Mater. Sci. Lett.* **1995**, *14*, 21−22.

(10) Trentler, T. J.; Denler, T. E.; Bertone, J. F.; Gagrawal, A.; Colvin, V. *J. Am. Chem. Soc.* **1999**, *121*, 1613−1614.

(11) Wang, C.-C.; Ying, J. Y. *Chem. Mater.* **1999**, *11*, 3113−3120.

(12) Kominami, H.; Takada, Y.; Yamagiwa, H.; Kera, Y. *J. Mater. Sci. Lett.* **1996**, *15*, 197−200.

(13) Cheng, H.; Ma, J.; Zhao, Z.; Qi, L. *Chem. Mater.* **1995**, *7*, 663−671.

(14) Yin, H.; Wada, Y.; Kitamura, T.; Sumida, T.; Hasegawa, Y.; Yanagida, S. *J. Mater. Chem.* **2002**, *12*, 378−383.

(15) Yanagisawa, K.; Ovenstone, J. *J. Phys. Chem. B* **1999**, *103*, 7781−7787.

(16) Zhang, Z.; Wang, C. C.; Zakaria, R.; Ying, J. Y. *J. Phys. Chem. B* **1998**, *102*, 10871−10878.

(17) Wu, Z. Y.; Zhang, J.; Ibrahim, K.; Xian, D. C.; Li, G.; Tao, Y.; Hu, T. D.; Bellucci, S.; Marcelli, A.; Zhang, Q. H.; Gao, L.; Chen, Z. Z. *Appl. Phys. Lett.* **2002**, *80*, 2973−2975.

(18) Almquist, C. B.; Biswas, P. *J. Catal.* **2002**, *212*, 145−156.

(19) Jung, K. Y.; Park, S. B.; Ihm, S.-K. *Appl. Catal.* **2002**, *224*, 229−237.

(20) Chen, L. X.; Rajh, T.; Wang, Z.; Thurnauer, M. C. *J. Phys. Chem. B* **1997**, *101*, 10688−10697.

(21) Martra, G. *Appl. Catal., A* **2000**, *200*, 275−285.

(22) Centi, G.; Ciambelli, P.; Perathoner, S.; Russo, P. *Catal. Today* **2002**, *75*, 3−15.

(23) Pirkanniemi, K.; Sillanpaa, M. *Chemosphere* **2002**, *48*, 1047−1060.

10.1021/la049334i CCC: $27.50
Published on Web 09/29/2004

Table 1. Synthetic Conditions for RHT Solvothermal Anatase Samples

sample	temperature (°C)	total volume (mL)	total [TEOT] (mol/L)	total [H_2O] (mol/L)	reaction time (h)
RHT 24	220	100	0.08	1.6	1.75
RHT 43	200	100	0.02	0.40	2
RHT 45	250	100	0.02	0.40	2
RHT 47	335	100	0.02	0.40	2
RHT 69	200	100	0.10	0.40	2
RHT 127	220	100	0.32	6.4	14

environmental pollutants that adsorb onto the particles. For example, the mobility of pollutants can often be enhanced or slowed by orders of magnitude because of the presence of colloidal particles in aquatic systems.[24−27]

Heavy metal contamination in natural environments has always been a great concern because heavy metals are toxic and nonbiodegradable. Adsorption onto oxides has been found to be important for many heavy metals and may significantly affect their mobility in aquatic environments. Laboratory experiments have demonstrated that titanium oxides (TiO_2) are strong sorbents for heavy metals.[28] In this study, the adsorptive interactions of Cd^{2+} with different sized anatase crystals have been studied over a pH range of 2−9. The objective of this study is to compare the adsorptive properties of a typical environmental pollutant onto large versus nanometer-scale anatase particles. Both commercial and laboratory synthesized anatase nanocrystals are compared to large-sized samples.

Materials and Methods

Four commercial anatase samples were used in this study. Two large-sized anatase crystal samples were from Sigma and Alfa Aesar. Two nanometer-scale anatase samples were from Altair (TiNano VHP-d) and Degussa (P-25). Reagent grade chemicals, for example, $Cd(NO_3)\cdot 4H_2O$, $NaNO_3$, NaN_3, and trace element grade nitric acid, were used in this study.

A process was developed for synthesizing nanocrystalline anatase with tunable grain sizes using solvothermal techniques in a neutral-pH environment. In a typical synthesis, a solution of water (Milli-Q UV-plus grade) in ethanol (200 proof, Pharmco Products) was heated with slow stirring to the desired reaction temperature in a 450-mL stainless steel pressure reactor (Parr Instruments, model 4562). Once the target temperature was reached, a solution of titanium(IV) ethoxide (TEOT; 97%, Avocado Research Products) in 200-proof ethanol was injected into the bomb and allowed to react for the desired amount of time. A cooling loop was used to quench the reactions. Products were filtered, washed with ethanol (190 proof, Pharmco Products), and centrifuged to isolate the TiO_2 powders, which were then allowed to dry in air for several hours. In Table 1 are listed the synthetic conditions for six different RHT samples. Comparison of samples RHT 43, 45, and 47 (synthesized at 200, 250, and 335 °C) indicates that higher reaction temperatures tend to yield larger grain sizes, which is consistent with previous reports in the literature.[11,13] TEOT and water concentrations also appear to play a role in determining grain size, but more experiments are needed to establish exactly how size depends on these parameters.

Solid-Phase Analysis. X-ray diffraction (XRD) spectra were taken using a Siemens platform-model general area detector diffraction system with a Cu Kα source at 50 kV and 40 mA. The sample-to-detector distance was set at 12.3 cm; the angular position of the detector with respect to the sample surface was set at 40°; and the collection time for each spectrum was 10−30 min. The RHT samples were run with an internal silicon powder standard to account for instrumental line broadening when calculating grain sizes from the anatase line widths.

Brunauer−Emmett−Teller (BET) surface areas were determined from N_2 adsorption onto the anatase powders using a Micromeritics ASAP 2010 apparatus. Samples were degassed for several hours at 150 °C prior to the N_2 adsorption analysis, which was carried out at liquid nitrogen temperature (−196 °C). Surface areas were obtained from a multipoint analysis of the volume of nitrogen adsorbed as a function of relative pressure.

Thermal gravimetry (TG) and differential thermal analysis (DTA) were performed on a Thermal Advantage SDT 2960 apparatus using a temperature range of 25−600 °C and a heating rate of 20 °C min^{-1}.

Transmission electron microscopy (TEM) was done on a JEOL 2010 apparatus equipped with a JEOL EM21010 single tilt stage. Each TEM sample was prepared by evaporating several drops of a dilute ethanol suspension of anatase powder onto a 300-mesh copper grid.

Potentiometric titrations of anatase suspensions were performed under nitrogen using a 0.1 mol/L aqueous solution of KNO_3 as the background electrolyte. Three anatase samples (TiNano, Sigma, and Alfa Aesar) were used in titration. To ensure comparable total surface areas among suspensions of the various samples, approximate solid concentrations of 2 and 7 g/L were used for the nanoscale sample (TiNano) and the coarser powders (Sigma and Alfa Aesar), respectively.

Before preparation of the anatase suspensions, powders were washed repeatedly with small portions (~25 mL) of the background electrolyte. The washed samples were dried at 90−100 °C under a vacuum and ground to fine powders using a mortar and pestle. An appropriate mass of each powder was then added to 100 mL of KNO_3 solution to give a suspension with the desired solid concentration.

Each suspension was equilibrated under nitrogen for at least 18 h before titration. After the suspension pH had reached an equilibrium value, a small amount (0.3−0.5 mL) of 0.0881 mol/L HNO_3 (standardized against 0.1 N NaOH) was added to the reactor. After an additional 15−20 min, the new equilibrium pH value was recorded as the initial pH. The suspension was then titrated with small aliquots (15−30 μL) of 0.0809 mol/L KOH (standardized against the HNO_3 solution) using a 100-μL Eppendorf micropipet. The pH was allowed to equilibrate after each addition and was then recorded as a function of the total volume of KOH titrant added.

Adsorption and Desorption Experiments. Cadmium adsorption was conducted with four nanometer-scale anatase samples (RHT 24, RHT 47, RHT 69, and RHT 127) prepared by the solvothermal method, two commercial nanometer-scale anatase samples (TiNano and P-25), and two large crystalline anatase samples (Sigma and Alfa Aesar). There was not enough of RHT 127 and 24 to measure a complete isotherm, but they were prepared to be similar to RHT 69 and, to a lesser extent, RHT 47, respectively. Adsorption studies were conducted in batch experiments.[29,30] In a typical experiment, anatase solid was weighed into a centrifuge bottle containing 40 mL of background electrolyte. A spike of concentrated Cd^{2+} (0.01 M) solution was added to initiate the adsorption. For adsorption isotherm studies, the Cd^{2+} concentrations used in these experiments ranged from 0 to 1.5 mM in a background electrolyte of 0.01 M $NaNO_3$, 0.01 M NaN_3, and 0.005 M MES (2-*N*-morpholino-ethanesulfonate) buffer at pH 6.1. The effect of MES buffer on Cd adsorption is presumably small because MES is known to have little tendency to bind metal ions.[31,32] The anatase solid concentrations were 5−25 g/L for Sigma and Alfa Aesar, 1.0−2.7 g/L for TiNano and P-25, and 0.5−0.7 g/L for all RHT samples. To maximize the

(24) Kan, A. T.; Tomson, M. B. *Environ. Toxicol. Chem.* **1990**, *9*, 253−263.
(25) Roy, S. B.; Dzombak, D. A. *Environ. Sci. Technol.* **1997**, *31*, 656−664.
(26) Kersting, A. B.; Efurd, D. W.; Finnegan, D. L.; Rokop, D. J.; Smith, D. K.; Thompson, J. L. *Nature* **1999**, *397*, 56−59.
(27) Honeyman, B. D. *Nature* **1999**, *397*, 23−24.
(28) Mishra, S. P.; Singh, V. K. *J. Radioanal. Nucl. Chem.* **1999**, *241*, 341−346.
(29) Kan, A. T.; Fu, G.; Tomson, M. B. *Environ. Sci. Technol.* **1994**, *28*, 859−867.
(30) Yin, Y.; Allen, H. E.; Huang, C. P. *Environ. Sci. Technol.* **1997**, *31*, 496−503.
(31) Good, N. E.; Winget, G. D.; Winter, W.; Connolly, T. N.; Izawa, S.; Singh, R. M. M. *Biochemistry (Moscow)* **1966**, *5*, 467−477.
(32) Good, N. E.; Izawa, S. *Methods Enzymol., Part B* **1972**, *24*, 53.

Table 2. Characterization of Different Anatase Samples

sample	crystalline phases detected by XRD	specific surface area (m^2/g)	mean particle size (nm)	amorphous TiO_2 detected by TG/DTA
Sigma	anatase	10.8[a] (8.3)	145[a]	none
Alfa Aesar	anatase	11.2[a] (9.5)	139.5[a]	none
TiNano	anatase	39.8[a] (39.4)	39.2[a]	none
P-25	anatase (80%), rutile (20%)	46.9[a] (50)	33.3[a]	none
RHT 47	anatase	75.1[b] (55.0)	20.8[b] (28.4)	none
RHT 24	anatase	108.5[b] (92.83)	14.4[b] (16.8)	
RHT 45	anatase		9.45	
RHT 43	anatase		7.72	
RHT 69	anatase	195.3[b] (149.2)	8.0[b] (10.5)	none
RHT 127	anatase	193.4[b] (130)	8.08[b] (12.0)	none

[a] Specific surface area is determined by nitrogen adsorption (BET surface area), and the particle size is estimated from the BET surface area. The numbers in parentheses are the corporate-literature-reported BET surface areas (Sigma, Alfa Aesar, Atlair, and Degussa). [b] Particle size and surface area are estimated from XRD data; the numbers in parentheses are the measured BET surface area and particle size estimated from BET surface area.

dispersion of anatase aggregates, the anatase−water mixtures were sealed and immersed in an ultrasonic bath for 30 min before being placed on a slowly rotating rack that provided gentle (40 rpm) end-over-end mixing for 24 h. At the end of each experiment, reaction tubes were centrifuged at 5000 rpm for 60 min, and the supernatant solutions were withdrawn with a syringe and filtered through 0.2-μm Nalgene syringe filters (SFCA) and 0.025-μm Millipore filters (type VS) for samples containing large and nanoscale anatase, respectively. The pH of each solution was measured immediately after sampling, and the filtrate was then acidified with 1% nitric acid and analyzed for solution Cd^{2+} concentrations. An UV−vis scan was performed on the filtered sample solutions using a HACH DR/4000V spectrophotometer; no absorption was observed in the 280−400 nm range, indicating the absence of anatase particles in the filtrates.

Successive adsorption experiments[33] were performed with the RHT 47 and RHT 69 samples. After the first adsorption experiment, another aliquot of Cd^{2+} stock solution (0.01 M) was added to the reaction vessel to initiate another step of the adsorption experiment. Cd^{2+} stock solution was successively added to the reaction vessel, and the adsorption experiment was repeated seven times. Successive desorption[30,33] experiments were run with Sigma, RHT 47, and RHT 69 samples after the adsorption experiment. Desorption was initiated by replacing 30 mL of supernatant solution with the background electrolyte solution, and the duration of each desorption step was 48 h. After a desorption step, the reaction vessel was centrifuged and ~30 mL of the supernatant was replaced with clean background electrolyte solution. This desorption step was repeated two times. For both adsorption and desorption experiments, the amount of Cd^{2+} adsorbed was calculated from the Cd^{2+} mass balance.

For the pH-dependent studies, similar Cd^{2+} adsorption experiments were conducted with RHT 127, Sigma, and TiNano samples at 25 °C. The pH of the solution was adjusted in the range 2−10 with either HNO_3 or KOH. The anatase concentrations were 10, 2.5, and 0.6 g/L for Sigma, TiNano, and RHT 127, respectively. At these solid−solution ratios, anatase surface areas per unit volume were similar (~100 m^2/L) for all experiments. The Cd^{2+} concentrations were ~0.2 mM for Sigma and TiNano samples and 0.1 mM for RHT samples.

An Orion Ross combination glass electrode and expandable ion analyzer EA 920 (Orion Research) were used for the pH measurements. The glass electrode was calibrated at 25 °C using buffers at pH of 4.0, 7.0, and 10.0. Solution-phase Cd concentrations were measured by ICP (Perkin-Elmer Optima 4000 DV) in a high concentration range ([Cd] > 0.1 mg/L) or ICP-MS (Perkin-Elmer Elan 9000) in a low concentration range ([Cd] < 100 μg/L). Cd was detected at a 228.802-nm wavelength with ICP or at 111 *m/e* with ICP-MS. ICP was calibrated at either 0−20 mg/L (radial mode) or 0−2 mg/L (axial mode) with standard Cd solutions, while ICP-MS was calibrated at 0−100 μg/L standard solutions in four to five point calibration. Yitium (at 10 mg/L and 371.029-nm wavelength for ICP or at 20 μg/L and 89 *m/e* for ICP-MS) was used as an internal standard for calibration. Excellent linear calibration is generally observed with a correlation coefficient of 0.9999 or better. A quality-control sample was analyzed every six samples to ensure that the calibration is valid for the analysis. The detection limit was 0.01 mg/L for ICP and 0.02 μg/L for ICP-MS, and the relative standard deviation of three replicate analyses was generally below 3%.

Results and Discussion

Physical Characterization of Anatase Samples. The physical characterization results of the various anatase samples are shown in Table 2. TG and DTA were used to assess the amorphous content of the anatase samples. A sharp exothermic peak in the 300−400 °C range, unaccompanied by weight loss, would have indicated crystallization of amorphous TiO_2 to anatase.[34] None of the powders exhibited this peak, and, therefore, the amorphous content of the samples may be assumed to be negligible. Each of the RHT samples did, however, exhibit a small, broad exothermic peak between 220 and 250 °C, most likely corresponding to the decomposition of residual organics. XRD results showed that all four RHT samples, Sigma, Alfa Aesar, and TiNano samples consisted of phase-pure anatase. Only P-25 showed a significant amount of rutile in addition to anatase phase. This is consistent with the literature report that P-25 contains 25−33% rutile, while the rest is mostly anatase.[18]

Particle size and surface area of nanoparticles are difficult to assess. We evaluated the particle size and surface area by both XRD analysis and the BET isotherm of nitrogen adsorption. Grain sizes for the RHT samples were estimated from XRD line widths according to the Debye−Scherrer formula with Warren's correction for instrumental broadening:[35]

$$D\ (\text{Å}) = 0.89\lambda/\beta \cos \theta_B \qquad (1)$$

where D is the crystallite size, λ is the X-ray wavelength (1.54 Å for Cu Kα radiation), θ_B is the Bragg angle, and $\beta \equiv (B^2 - b^2)^{1/2}$ where B and b are taken as the full width at half-maximum of, respectively, the [101] line of anatase ($2\theta = 25.4°$) and the [111] line of the silicon standard ($2\theta = 28.3°$). XRD spectra for RHT 69 and RHT 47 samples are shown in Figure 1; the narrower lines in the lower spectrum correlate with a larger grain size (~20 nm, RHT 47), while the more pronounced line broadening in the upper spectrum indicates a smaller grain size (~8 nm, RHT 69). Because line broadening due to size effects is

(33) Kan, A. T.; Fu, G.; Hunter, M. A.; Tomson, M. B. *Environ. Sci. Technol.* **1997**, *31*, 2176−2185.

(34) Kondo, M.; Shinozaki, K.; Ooki, R.; Mizutani, N. *J. Ceram. Soc. Jpn.* **1994**, *102*, 740−744.

(35) Klug, H. P.; Alexander, L. E. *X-Ray Diffraction Methods for Polycrystalline and Amorphous Materials*; John Wiley and Sons: New York, 1954.

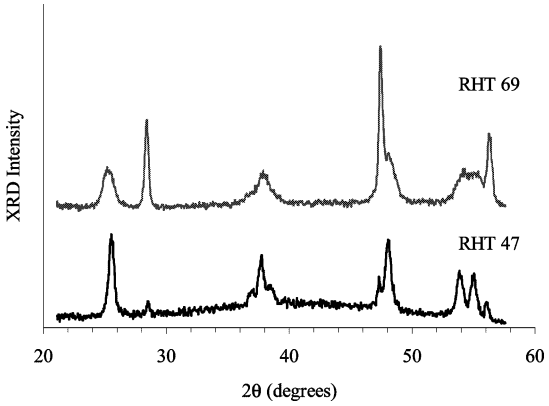

Figure 1. Plot of the XRD patterns of two nanoparticle-sized anatases, RHT 69 and RHT 47. The peak broadening at $2\theta = 25.4$ is used to calculate the particle diameter via eq 1.

only significant for very small crystallites, grain size determination from XRD line widths was not feasible for the commercial samples, all of which are coarser than the RHT powders.

Particle diameters for all samples were also calculated from the BET surface areas assuming spherical particles and a density of ρ(anatase) = 3.84 g cm^{-3}. For the very small nanoparticles (RHT samples), the particle sizes determined from the BET surface area were somewhat larger than the grain sizes estimated from the XRD line widths. This difference may be partly attributable to aggregation among individual crystallites, which would reduce the surface area available for N_2 adsorption and, in turn, yield surface area measurements corresponding to larger grain sizes. The TEM image shown in Figure 2a confirms that there was indeed some aggregation in the RHT samples. However, it should also be noted that aggregation was also observed in the TiNano and Alfa Aesar samples (parts b and c of Figure 2, respectively), yet the experimental BET surface areas for these samples were either equal to (TiNano) or larger than (Alfa Aesar) the values reported in the literature. Therefore, aggregation cannot completely account for the observed discrepancies between the BET- and the XRD-derived surface areas for the RHT samples. An alternative explanation might be that the RHT sample sizes in the BET experiments were very small (<50 mg), which could have introduced or exacerbated inaccuracies in the measurements for those samples.

In Table 2, column 3, are listed the measured BET surface area for the commercial anatase samples and the measured XRD surface area for the RHT samples. The surface areas reported here are used for analysis of the adsorption data below. The corporate-literature-reported BET surface areas for the commercial samples, as well as the laboratory measured BET surface area for the RHT samples, are also listed in the parentheses of column 3 for comparison.

Potentiometric Titrations of Anatase. In Figure 3 is plotted the surface charge, σ, versus pH for three anatase samples (TiNano, Alfa Aesar, and Sigma). The surface charge, σ, of each anatase sample was calculated as a function of pH from potentiometric titration according to eq 2:[36]

$$\sigma\,(\mathrm{C\ m^{-2}}) = F(C_a - C_b - [\mathrm{H^+}] + [\mathrm{OH^-}])W^{-1}S^{-1} \quad (2)$$

where F is the Faraday constant (96 485 C/mol), C_a and C_b are the total concentrations of acid and base, respectively (mol/L), [H$^+$] is the proton concentration (mol/L) given by $10^{-\mathrm{pH}}/\gamma_{\mathrm{H}^+}$, [OH$^-$] is the OH$^-$ concentration (mol/L) given by $10^{-(\mathrm{p}K_w-\mathrm{pH})}/\gamma_{\mathrm{OH}^-}$, W is the anatase concentration (g L^{-1}), and S is the specific surface area (m^2 g^{-1}).[36] The activity coefficient of H$^+$ and OH$^-$, γ_{H^+} and γ_{OH^-} (=0.776), is estimated from Davis equation at 0.1 M ionic strength.[36] C_a and C_b are calculated from the normality of acid/base and total volume of the solution at each titration point, as illustrated by Ludwig and Schindler.[37] Note that anatase is relatively insoluble between pH 3 and pH 9[38] and correction for anatase solubility is not needed. Through out the range of pH values in these experiments (pH 3−9) and 0.1 M KNO_3, anatase solubility is approximately 1.75×10^{-7} M because the predominant species in solution is $Ti(OH)_4^{\pm 0}$ which is electronically neutral. This was calculated using VisualMINTEQ, version 2.30, 2004, for rutile and using the difference in the free energy of formation from rutile to antase to calculate the solubility of anatase. Plots of σ against pH (Figure 3) were used to compare the acid−base behavior of the different sample surfaces. The point of zero charge (pzc) is the pH value at which $\sigma = 0$. All three anatase powders were found to have pzc values of 6.0−6.1 pH, which is in good agreement with the values reported in the literature.[39−41] The titration curves, when normalized to the unit surface area as shown in Figure 3, are virtually identical for all three anatase samples, suggesting that there is no appreciable difference in the surface acid−base properties of large and nanometer-scale anatase.

Adsorption of Cadmium to Anatase Samples. Adsorption isotherms are plotted in Figure 4. The adsorption data are grouped by their size and source. In Figure 4a,b are the adsorption data of large anatase crystals (Sigma and Alfa Aesar). The specific surface area for these two samples is ~11 m^2/g. In Figure 4c,d are the adsorption data of commercial-nanoparticle-sized anatase (P-25 and TiNano). These two nanomaterials are about 30−40 nm in size, and the specific surface area is in the range of 40−47 m^2/g. Note that P-25 is 75% anatase and 25% rutile. Cd adsorption to either P-25 or TiNano is very similar. The pzc for rutile is pH 5.3 versus pH 6.2 for anatase.[38] The similarity in Cd adsorption to P-25 and TiNano indicates that Cd adsorption to anatase is primarily electrostatic driven. In Figure 4e,f are the adsorption data of RHT samples prepared in our laboratory. The RHT nanoparticles are considerably smaller (8−20 nm) than the commercial nanoparticles and have a significantly larger specific surface area (75−195 m^2/g). In Figure 4a,c,e is plotted the weight-based solid-phase concentration versus solution-phase concentration, and in Figure 4b,d,f is plotted the surface area normalized solid-phase concentration versus solution-phase concentration. RHT 24 is a sample prepared in a preliminary study. RHT 127 has physical characteristics very similar to those of RHT 69. Only single-point adsorption experiments were done on these two laboratory prepared anatase samples due to limited sample amounts. The single-point adsorption data for RHT 24 (10-nm particle size) and RHT 127 (8-nm

(36) Stumm, W.; Morgan, J. J. *Aquatic Chemistry: Chemical Equilibria and Rates in Natural Waters*, 3 ed.; John Wiley & Sons, Inc.: New York, 1996.
(37) Ludwig, C.; Schindler, P. W. *J. Colloid Interface Sci.* **1995**, *169*, 284−290.
(38) Parfitt, G. D. *Prog. Surf. Membr. Sci.* **1976**, *11*, 181−226.
(39) Janusz, W.; Jablonski, J.; Sprycha, R. *J. Dispersion Sci. Technol.* **2000**, *21*, 739−759.
(40) Weng, C. H.; Wang, J. H.; Huang, C. P. *Water Sci. Technol.* **1997**, *35*, 55−62.
(41) Rodriguez, R.; Blesa, M. A.; Regazzoni, A. E. *J. Colloid Interface Sci.* **1996**, *177*, 122−131.

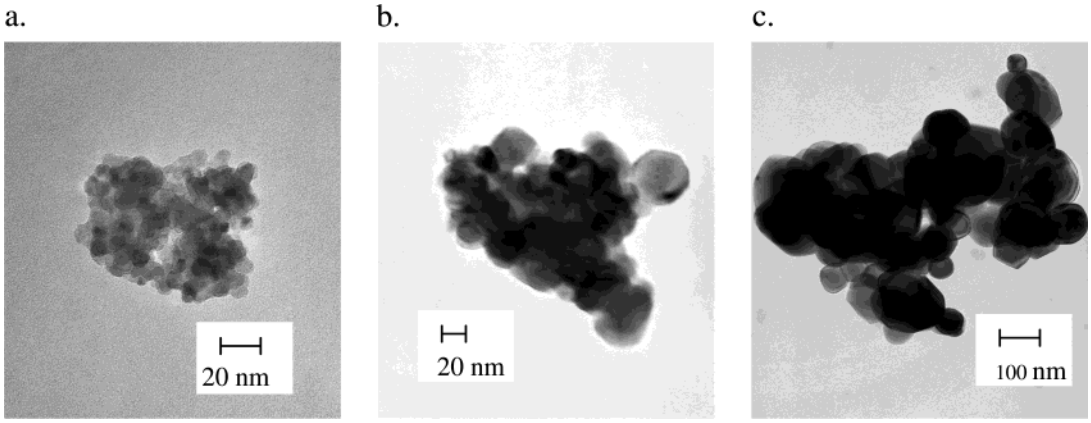

Figure 2. TEM images of (a) RHT 69; (b) TiNano; and (c) Alfa Aesar anatase.

Table 3. Weight-Based Langmuir Adsorption Isotherm Parameters

solid	Q_{max} (μmol/g)	b (mL/μmol)	$Q_{max}b$ (mL/g)	$\sigma_{Q_{max}}{}^b$ (mL/g)	$\sigma_b{}^b$ (mL/μmol)	r^b
Sigma and Alfa Aesar[a]	34.95	100.5	3512.47	1.41	27.4	0.978
P-25	179.15	3.61	646.55	5.53	0.24	0.998
TiNano	141.58	3.27	463.11	5.23	0.47	0.984
RHT 47	244.13	8.94	182.5	11.55	1.33	0.991
RHT 69	497.90	7.71	3838.8	23.40	1.06	0.991

[a] The adsorption data for Sigma and Alfa Aesar are fitted together with a single Langmuir isotherm. [b] σ is one standard deviation of the parameters, Q_{max} and b, determined by the PSI-Plot fit of eq 3 to the experimental data. r is the correlation coefficient of the data fitted by the model, eq 3.

Table 4. Surface-Area-Normalized Langmuir Adsorption Isotherm Parameters

solid	Q_{max} (μmol/m^2)	b (mL/μmol)	$Q_{max}b$ (mL/m^2)	$\sigma_{Q_{max}}{}^c$ (mL/m^2)	$\sigma_b{}^c$ (mL/μmol)	r^c
Sigma and Alfa Aesar[a]	3.19	108.7	346.75	0.12	29.2	0.978
P-25 and TiNano[b]	3.50	3.70	12.94	0.10	0.40	0.985
RHT 47	3.25	8.94	29.02	0.15	1.33	0.991
RHT 69	2.55	7.71	19.7	0.12	1.06	0.991

[a] The adsorption data for Sigma and Alfa Aesar are fitted together with a single Langmuir isotherm. [b] The adsorption data for P-25 and TiNano are fitted together with a single Langmuir isotherm, see Figure 4d. [c] σ is one standard deviation of the parameters, Q_{max} and b, determined by the PSI-Plot fit of eq 3 to the experimental data. r is the correlation coefficient of the data fitted by the model, eq 3.

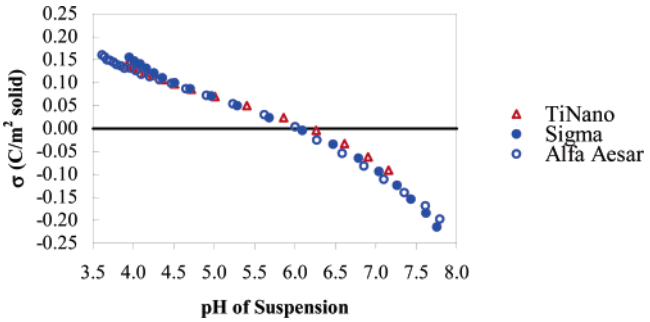

Figure 3. Potentiometric titration curves for nanoparticle-sized (TiNano, open triangles) and large (Sigma, Alfa Aesar, open and filled circles) anatase samples.

particle size) are similar to that of RHT 69 in both the weight-based and surface-area-normalized plots (Figure 4e,f).

All adsorption data were fitted with a Langmuir isotherm (the lines, eq 3):

$$q\ (\mu\text{mol/g or } \mu\text{mol/m}^2) = \frac{bQ_{max}\text{C}\ (\mu\text{mol/mL})}{1 + bC\ (\mu\text{mol/mL})} \quad (3)$$

where Q_{max} (μmol/g or μmol/m^2) is the maximum sorption capacity of the solid and b is the sorption constant related to the adsorption energy (mL/μmol). Both Langmuir parameters were determined by fitting eq 3 to experimental data using the PSI-Plot program. Note that a good fit of the data to the Langmuir isotherm does not constitute evidence that adsorption satisfies the criteria of the adsorption model.[42] If the adsorption pH is significantly different from the pzc, a more complicated isotherm would be required, such as a Frumkin−Fowler−Guggenheim interaction equation.[42,43] The adsorption isotherms of Sigma and Alfa Aesar are very similar. The data in Figure 4a,b are fitted with a single isotherm. The curve-fitted Langmuir parameters, standard deviation of the parameters, and correlation coefficients are listed in Tables 3 and 4. In Table 3 are listed the weight-based Langmuir parameters (Q_{max}, μmol/g). A very good fit of the experimental data to a Langmuir isotherm was observed for all six anatase samples. As expected, the weight-based Cd^{2+} adsorption capacity (Q_{max}, μmol/g) was larger for the smaller nanoparticles with higher surface area (Table 3). At pH 6.1, on a per-mass basis, the Cd^{2+} maximum adsorption capacity was 498 μmol/g for RHT 69 and 35 μmol/g for the large crystals.

In Table 4 are listed the surface-area-based Langmuir parameters (Q_{max}, μmol/m^2). Because the adsorption isotherms of TiNano and P-25 are nearly identical after normalization to the surface area (Figure 4d), the data in Figure 4d are fitted with a single Langmuir isotherm. Interestingly, the surface-area-normalized Cd^{2+} adsorption capacities are very similar (2.55−3.50 μmol/m^2, Table 4). The highest adsorption capacity is observed with the

(42) Tamura, H., Hubbard, A. T., Eds. *Encyclopedia of Surface and Colloid Science*; Marcel Dekker: New York, 2002; pp 2856−2875.
(43) Stumm, W. *Chemistry of the Solid-Water Interface*; John Wiley and Sons: New York, 1992.

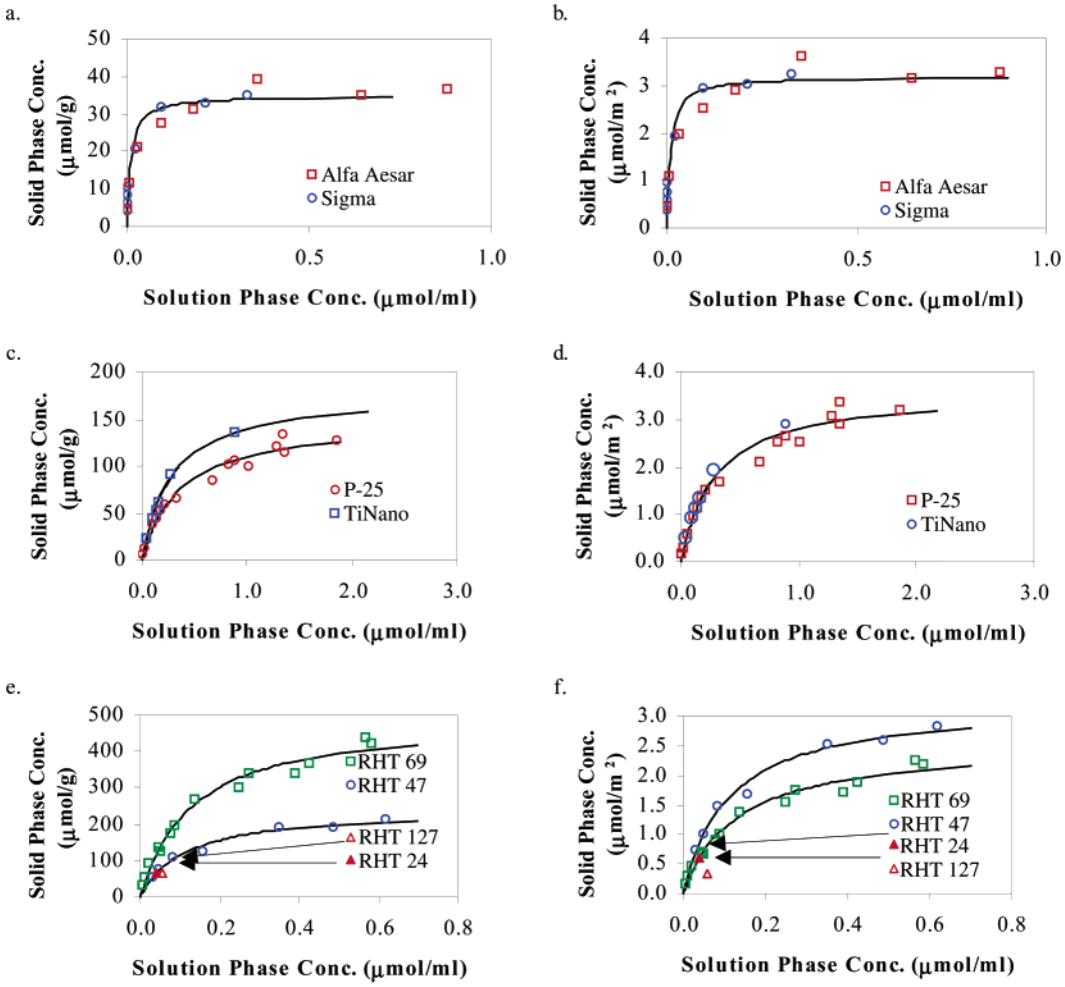

Figure 4. Plot of the adsorption isotherm of Cd^{2+} to eight different anatase solids at pH 6.1 and 25 °C. (a, b) Large anatase crystals (Sigma and Alfa Aesar); (c, d) commercial nanoparticle-sized anatase (TiNano and P-25); and (e, f) RHT samples (RHT 69 and RHT 47). In plots e and f, the single-point adsorption data for RHT 24 (solid triangle) and RHT 127 (open triangle) are also plotted. In the three plots on the left-hand side (a, c, and e) are plotted the weight-based solid-phase Cd^{2+} concentrations (μmol/g) versus the solution-phase Cd^{2+} concentrations (μmol/mL), and in the three plots on the right-hand side (b, d, and f) are plotted the surface-area-normalized solid-phase Cd^{2+} concentrations (μmol/m^2) versus the solution-phase Cd^{2+} concentrations (μmol/mL). The lines are the Langmuir isotherm fits of the adsorption data. The Langmuir parameters are listed in Tables 3 and 4.

30−40-nm commercial nanometer-scale anatase (TiNano and P-25). The adsorption capacities for the large crystals (Sigma and Alfa Aesar) and the 20-nm anatase nanoparticles (RHT 47) are similar. The adsorption capacity of the 8-nm RHT 69 anatase is significantly smaller than that of all other anatase samples. Note that the measured and literature-reported BET surface areas for the two commercial nanoparticle-sized anatases (TiNano and P-25) are quite consistent, while the measured and literature-reported BET surface areas for the two large anatase crystal samples (Sigma and Alfa Aesar) differ. Therefore, the surface area normalized adsorption capacities for the large anatase crystals (Sigma and Alfa Aesar) and 30−40 nm particles (TiNano and P-25) could be similar. Additionally, there are some discrepancies between the BET and XRD-derived surface areas for the RHT 47 sample. Therefore, the Cd^{2+} adsorption capacity may not be different among these anatase samples with grain sizes greater than 20 nm (Sigma, Alfa Aesar, TiNano, P-25, and RHT 47). The adsorption capacity of the RHT 69 is slightly smaller than those of the other anatase samples, even if the lower BET surface area is assumed in calculation of the surface area normalized capacity. The Langmuir adsorption capacity corresponds to a Cd^{2+} adsorption density of 47−65 Å^2/Cd^{2+} ion or about 2 sites/1 nm^2. This is consistent with results reported by Robertson and Leckie[44] and Vassileva et al.[45] Interestingly, this corresponds to a potentially countable number of Cd^{2+} ions per nanoparticle for some of the smaller particles.

The most noticeable difference between the large and nanoscale crystals is in the *b* term of the Langmuir isotherm (Table 4, Column 3). These data indicate a significant difference between the sorption energies for Cd^{2+} to large versus small anatase crystals. The *b* term only varied by a factor of 2−3 among the commercial and laboratory prepared nanometer-scale anatase samples, but the *b* term for the larger anatase samples was 10−30 times larger than the nanoparticles. The *b* term in the Langmuir isotherm (eq 3) represents the equilibrium constant for adsorption when all concentrations are expressed as mole fractions.[46] Some of these nanoparticles are similar in size to large globular proteins, as discussed by Tanford,[47] and the reduced *b* values may be due to intraparticle electrostatic interactions as a result of increased Cd^{2+} adsorption. Bodek et al.[48] compiled a range of Cd^{2+} adsorption values to oxides and natural sediments.

(44) Robertson, A. P.; Leckie, J. O. *J. Colloid Interface Sci.* **1997**, *188*, 444−472.
(45) Vassileva, E.; Proinova, I.; Hadjiivanov, K. *Analyst (Cambridge, U.K.)* **1996**, *121*, 607−612.
(46) Adamson, A. W.; Gast, A. P. *Physical Chemistry of Surfaces*, 6th ed.; John Wiley & Sons: New York, 1997.

Table 5. Adsorption of Cd^{2+} to Three Different Anatase Crystals at Various pHs

solid	anatase concn (g/L)	pH	C_{init} (μmol/mL)	C (μmol/mL)	q_{ads} (μmol/g)	q_{ads} (μmol/m^2)	log K_d[a]
Sigma	10.0	2.17	0.199	0.1861	1.330	0.123	−0.179
Sigma	10.1	3.47	0.195	0.1582	3.712	0.344	0.337
Sigma	10.0	3.7	0.192	0.1537	4.002	0.371	0.382
Sigma	10.2	3.99	0.199	0.1438	5.515	0.511	0.550
Sigma	10.0	4.78	0.199	0.1176	8.121	0.752	0.806
Sigma	10.0	4.98	0.199	0.0865	11.159	1.033	1.077
Sigma	10.0	5.38	0.200	0.0885	11.198	1.037	1.069
Sigma	10.0	5.8	0.200	0.0325	16.758	1.552	1.680
Sigma	10.1	6.2	0.199	0.0137	18.438	1.707	2.097
Sigma	10.0	6.51	0.205	0.0070	19.465	1.802	2.411
Sigma	10.2	6.7	0.202	0.0041	19.236	1.781	2.641
Sigma	10.1	7.14	0.200	0.0018	19.680	1.822	3.018
Sigma	10.0	7.29	0.202	0.0012	19.882	1.841	3.182
Sigma	10.1	7.53	0.201	0.0007	19.763	1.830	3.443
Sigma	10.0	8.31	0.202	0.0001	20.179	1.868	4.276
Sigma	10.2	9.18	0.199	0.0001	19.626	1.817	4.356
TiNano	2.5	3.7	0.202	0.195	2.723	0.068	−0.455
TiNano	2.5	3.95	0.198	0.192	2.590	0.065	−0.469
TiNano	2.6	4.38	0.196	0.188	2.911	0.073	−0.411
TiNano	2.5	4.79	0.195	0.185	3.788	0.095	−0.290
TiNano	2.7	5.03	0.196	0.174	8.393	0.211	0.082
TiNano	2.5	5.42	0.197	0.182	5.679	0.143	−0.107
TiNano	2.6	5.8	0.206	0.151	21.165	0.532	0.547
TiNano	2.5	6.01	0.199	0.112	34.004	0.854	0.881
TiNano	2.5	6.14	0.195	0.098	38.980	0.979	1.000
TiNano	2.5	6.18	0.196	0.094	40.281	1.012	1.030
TiNano	2.5	6.28	0.198	0.077	47.581	1.196	1.194
TiNano	2.5	6.3	0.197	0.073	48.719	1.224	1.222
TiNano	2.5	6.31	0.196	0.077	48.192	1.211	1.197
TiNano	2.5	6.36	0.195	0.070	49.868	1.253	1.256
TiNano	2.5	6.37	0.201	0.068	51.640	1.297	1.279
TiNano	2.5	6.5	0.200	0.058	56.900	1.430	1.389
TiNano	2.5	6.83	0.200	0.032	66.786	1.678	1.722
TiNano	2.5	6.87	0.202	0.030	68.240	1.715	1.752
TiNano	2.5	7.15	0.198	0.017	72.490	1.821	2.035
TiNano	2.5	7.55	0.202	0.006	77.720	1.953	2.529
TiNano	2.5	9.95	0.205	0.000	81.211	2.040	5.009
TiNano	2.5	10	0.198	0.000	79.393	1.995	4.601
RHT127	0.6	4.84	0.104	1.04×10^{-1}	0.213	0.001	−1.974
RHT127	0.6	5.49	0.105	8.25×10^{-2}	35.585	0.184	0.348
RHT127	0.7	5.98	0.105	5.91×10^{-2}	65.179	0.337	0.756
RHT127	0.6	6.64	0.105	1.56×10^{-2}	141.151	0.730	1.669
RHT127	0.6	6.66	0.105	1.70×10^{-2}	142.241	0.735	1.636

[a] $K_d = q_{ads}$ (μmol/m^2)/C (μmol/mL), single-point distribution coefficient.

The b terms for Cd^{2+} adsorption are 10^3 (mL/μmol) for Fe oxides, $10^{1.0-3.3}$ (mL/μmol) for Mn oxides, and $10^{3.8-4.0}$ (mL/μmol) for montmorillonite clay (pH 5−8.5). The b term for Cd^{2+} adsorption to large anatase crystals is $10^{2.03}$ (mL/μmol), which is similar to the Cd^{2+} adsorption energy to Mn oxides, while the b terms for Cd^{2+} adsorption to the nanoparticle-sized anatase particles ($10^{0.54}$−$10^{0.95}$ mL/μmol) are significantly lower than all of these previously reported values.

Hysteretic desorption has been reported for many gas−solid and liquid−solid interactons.[33,46,49−51] Therefore, the reversibility of Cd^{2+} desorption from anatase samples was studied to determine if the nanoparticle-sized anatase particles exhibit unusual desorption behavior. In Figure 5 is plotted the surface-area normalized adsorption/desorption isotherm of Cd^{2+} from two nanometer-scale (RHT 47 and 69) and large (Sigma) anatase samples at pH 6.1. The desorption of cadmium from both large and nanometer-scale anatase particles appears to be completely reversible, indicating that no unusual adsorption/desorption behavior should be expected.

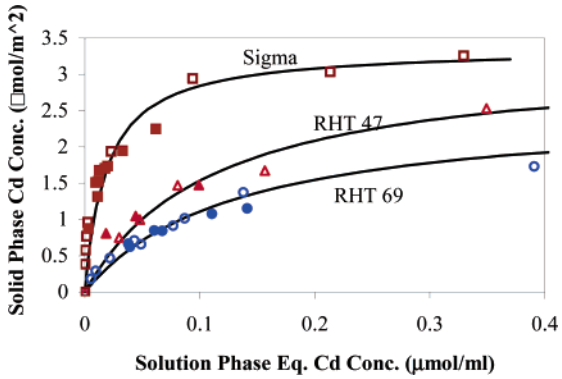

Figure 5. Plot of the adsorption/desorption isotherm of Cd^{2+} to large anatase (Sigma) and two nanocrystalline anatases (RHT 47 and RHT 69) at pH 6.1 and 25 °C. The open symbols are data from the adsorption approach and the closed symbols are data from the desorption approach.

In Table 5 are listed the experimental results of single-point Cd^{2+} adsorption at various pH values for Sigma, TiNano, and RHT 127. Note that the initial Cd concentration will be supersaturated with respect to the Cd-$(OH)_2$ phase at pH > 9. The possibility of $Cd(OH)_2$

(47) Tanford, C. *Physical Chemistry of Macromolecules*; John Wiley & Sons: New York, 1967.
(48) Bodek, I., Lyman, W. J., Reehl, W. F., Rosenblatt, D. H., Eds. *Environmental Inorganic Chemistry*; Pergamon Press: New York, 1988.
(49) Everett, D. H.; Whitton, W. I. *Trans. Faraday Soc.* **1952**, *48*, 749−757.
(50) Yin, Y.; Allen, H. E.; Huang, C. P.; Sanders, P. F. *Soil Sci.* **1997**, *162*, 35−45.
(51) Ainsworth, C. C.; Pilou, J. L.; Gassman, P. L.; Sluys, W. G.; Cobalt, V. D. *Soil Sci. Soc. Am. J.* **1994**, *58*, 1615.

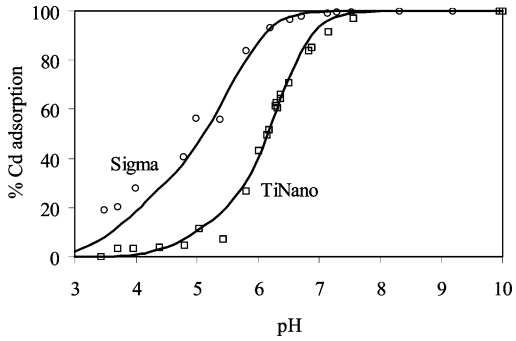

Figure 6. Plot of the % Cd adsorption versus pH at 25 °C. The initial Cd^{2+} concentrations are 200 μM for Sigma (○) and TiNano (□) experiments. The anatase solid concentrations are 10 and 2.5 g/L for Sigma and TiNano, respectively, which yield the anatase surface area concentrations of ~100 m^2/L for all experiments. BSM model fits including three surface complexes are represented by the solid lines.

precipitation at pH > 9 cannot be ruled out. However, the adsorption of Cd by anatase is very strong at pH 9 and the residual Cd concentration is significantly below the solubility of the $Cd(OH)_2$ phase. At extreme pHs, the solution ionic strength may change slightly but it shall not affect the results significantly. Anatase is not very soluble between pH 2−10. As a result of the limited RHT 127 sample size, the pH range tested for RHT 127 was limited to pH 4.8−6.7. Because it is difficult to produce a large quantity of RHT nano-TiO_2, the surface acid−base properties of other RHT nanoparticles have not yet been established. In Figure 6 is plotted the Cd^{2+} adsorption edge versus pH for Sigma and TiNano data. As shown in Figure 6, cadmium displays a typical adsorption edge for multivalent cations and shows a strong affinity for both the Sigma and TiNano anatase surfaces. A similar pH dependence of cadmium adsorption has been observed on titanium oxide by other researchers.[28,39] The pH dependences of the adsorption of Cd^{2+} to nanoparticle-sized (TiNano, RHT 127) and large (Sigma) anatase samples are similar, except that the adsorption to large crystals is much stronger than adsorption to nanoparticle-sized particles throughout the pH range. The amount of Cd^{2+} adsorbed onto both nanoparticle-sized and large anatase crystals increases when the pH is increased from pH 4 to 9.

The distribution coefficient, K_d (mL/m^2), is used to assess cadmium adsorption at a specific set of solution conditions and is defined by eq 4:

$$K_d\ (\text{mL/m}^2) = q_{ads}\ (\mu\text{mol/m}^2)/C\ (\mu\text{mol/mL}) \qquad (4)$$

At low concentrations of Cd^{2+}, the Langmuir isotherm reduces to a linear isotherm with a distribution coefficient (K_d) equal to the product of $Q_{max}b$ and it is this quantity which is central to predicting transport.[36] The term $Q_{max}b$ represents the slope of the linear portion of the Langmuir isotherm. In Figure 7 is plotted the logarithm of the distribution constant versus pH for the pH range 4−7.5. The log K_d versus pH curves are essentially parallel for Sigma and TiNano between pH 4 and pH 7.5, and, therefore, the ratio of adsorption for Sigma to TiNano is approximately constant over this pH range. The log K_d versus pH plot for RHT 127 coincides with the TiNano data, which supports the previous conclusion that the adsorption energies for the nanoscale particles are similar, and there appears to be no systematic difference between the commercial TiNano material and the RHT 127 prepared in our laboratory. On a "per surface area" basis,

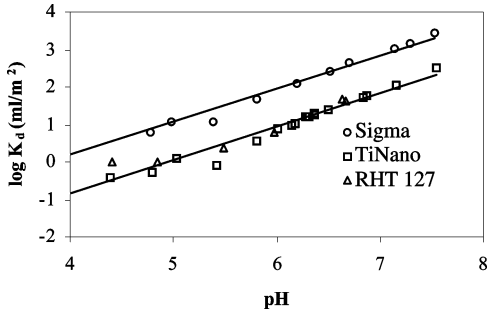

Figure 7. Plot of the logarithm of the single-point distribution coefficient, K_d (mL/m^2), versus pH for the adsorption of Cd^{2+} to Sigma, TiNano, and RHT 127 anatase samples at various pHs and 25 °C.

the adsorption of Cd^{2+} to anatase is 10−33 times larger for the large crystals than for the nanoparticle-sized crystals.

Surface Complexation Model. We used the Basic Stern model (BSM) to describe Cd^{2+} adsorption to Sigma and TiNano anatase.[52−54] The model was not extended to RHT data because of limited knowledge regarding RHT surface acid−base and adsorption properties. Therefore, the resulting model may not be applicable to RHT particles. The basic assumptions of surface complexation models are probably not strictly valid for nanometer-sized particles, but they provide a common frame of reference to report adsorption equilibrium constants for metal oxides. Such a double layer model is commonly used to describe adsorption to small nanocrystals, for example, ferrihydrates with specific surface areas in excess of 600 m^2/g.[53] In our modeling, we characterized the acid−base properties of the anatase surface using the two classical surface acidity constants, pK's. The acid−base properties of the surface are described by the following two reactions and corresponding mass action laws:

$$>\text{TiOH} + \text{H}^+ = >\text{TiOH}_2^+ \qquad (5)$$

$$>\text{TiOH} = >\text{TiO}^- + \text{H}^+ \qquad (6)$$

where > represents surface species. This 2-pK model is based on the assumption that the anatase surface is homogeneous with only one type of active surface functional group. In the present study, results of cadmium adsorption on anatase were treated using the BSM with the aid of the computer program Fiteql, version 4.0.[55] Fiteql is used extensively for the determination of chemical equilibrium constants in adsorption studies.[56−62] Cadmium

(52) Stumm, W.; Morgan, J. J. *Aquatic Chemistry Chemical Equilibriua and Rates in Natural Water*, 2nd ed.; Wiley-Interscience: New York, 1996.
(53) Dzombak, D. A.; Morel, F. M. M. *Surface Complexation Modeling, Hydrous Ferric Oxide*; John Wiley & Sons: New York, 1990.
(54) Westall, J.; Hohl, H. *Adv. Colloid Interface Sci.* **1980**, *12*, 265−294.
(55) Herbelin, A.; Westall, J. C. *Fiteql: A Computer Program for Determination of Chemical Equilibrium Constants from Experimental Data*, version 4.0; Oregon State University: Corvallis, OR, 1999.
(56) Goldberg, S. *Soil Sci. Soc. Am. J.* **1985**, *49*, 851−856.
(57) Lovgren, L.; Sjoberg, S.; Schindler, P. W. *Geochim. Cosmochim. Acta* **1990**, *54*, 1301−1306.
(58) Hayes, K. F.; Redden, G.; Ela, W.; Leckie, J. O. *J. Colloid Interface Sci.* **1991**, *142*, 448−469.
(59) Gunneriusson, L. *J. Colloid Interface Sci.* **1994**, *163*, 484−492.
(60) Boily, J. F.; Fein, J. B. *Geochim. Cosmochim. Acta* **1996**, *60*, 2929−2938.
(61) Daughney, C. J. *Selected Geochemical Reactions in Heavy Metal-Chlorophenol Systems*. Ph.D. Thesis, McGill University, Montreal, Quebec, Canada, 1997.
(62) Gao, Y.; Mucci, A. *Geochim. Cosmochim. Acta* **2001**, *65*, 2361−2378.

Table 6. Summary of Surface Complexation Reactions and Intrinsic Equilibrium Constants Describing Cadmium Adsorption at the Surface of Sigma and TiNano Anatase Using the BSM

component reaction	Sigma (log *K*)	TiNano (log *K*)
$>TiOH + H^+ = >TiOH_2^+$	4.98[a]	4.98[a]
$>TiOH = >TiO^- + H^+$	7.80[a]	7.80[a]
$>TiOH + Cd^{2+} = >TiOHCd^{2+}$	6.38 (0.04)[b]	4.26 (0.06)[b]
$>TiOH + Cd^{2+} = >TiOCd^+ + H^+$	−8.10 (0.05)[b]	−9.10 (0.08)[b]
$>TiOH + Cd^{2+} = >TiOCdOH^0 + 2H^+$	−0.04 (0.15)[b]	−2.15 (0.04)[b]
total sites (mmol L^{-1})	0.39[c]	0.36[c]
particle concentration (g L^{-1})	10	2.5
specific capacitance (F m^{-2})	1.6	3.0

[a] Values were taken from Parfitt.[38] [b] Values in parentheses are the standard deviation of the parameters calculated by Fiteql.[55] [c] Values were calculated as the product of the specific surface area (m^2/g), capacity (μmol/m^2), and particle concentration (g/L). The specific surface area (m^2/g) and capacity (μmol/m^2) are listed in Tables 2 and 4, respectively.

complexation constants at the anatase surface can be obtained using the total concentration of adsorbed cadmium and pH as governing parameters. The concentration of the total surface sites was calculated on the basis of the specific surface area listed in Table 2, the maximum adsorption capacity listed in Table 4, and the anatase concentration listed in Table 5. The surface acidity constants of anatase of Parfitt[38] were used.

Cadmium ions may form various monodentate surface complexes or bidentate surface complexes according to the following reactions listed below (eqs 7−10):

$$>TiOH + Cd^{2+} = >TiOHCd^{2+} \quad (7)$$

$$>TiOH + Cd^{2+} = >TiOCd^+ + H^+ \quad (8)$$

$$>TiOH + Cd^{2+} + H_2O = >TiOCdOH^0 + 2H^+ \quad (9)$$

$$2>TiOH + Cd^{2+} = (>TiO^-)_2Cd^{2+} + 2H^+ \quad (10)$$

In Table 6 are listed the anatase complexation constants for reactions 7−9 as well as other modeling parameters. In Figure 6 is plotted the BSM model fit (the lines) to experimental data. In our modeling, different combinations of monodentate and bidentate complexes were tested. The best fit to the experimental data was obtained with a BSM comprising three monodentate surface complexes, the formation reactions for which are described by eqs 7−9 (Figure 6). Models including only one or any combination of two of the three monodentate complexes result in poorer fits to the experimental data. Similarly, Gunneriusson[59] reported that a model including three surface complexes (>FeOHCd^{2+}, >FeOCd$^+$, and >FeOCdOH^0) successfully reproduced cadmium adsorption on goethite. Ludwig and Schindler[37] also used a three-surface-complex model to represent their data on copper adsorption by anatase.

Clearly, our model reproduces cadmium adsorption data successfully (Figure 6). On the basis of the complexation reactions and the corresponding equilibrium constants in Table 6, the surface speciation of Cd^{2+} adsorption on anatase as a function of pH is shown in Figure 8. Generally, cadmium surface speciation on both Sigma and TiNano anatase follows a similar trend: $>TiOHCd^{2+}$ is the dominant surface complex at low pH, $>TiOCd^+$ and $>TiOCdOH^0$ become the important species at circumneutral pH, and $>TiOCdOH^0$ is the most abundant surface species at higher pH. Nevertheless, the relative importance of three surface species appear different for these two

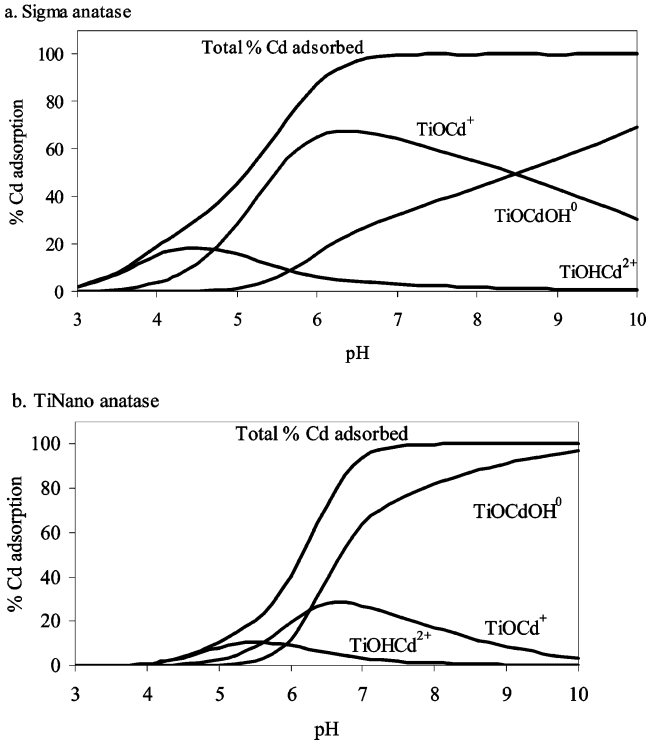

Figure 8. BSM model predictions of the distribution of cadmium species at the surface of anatase.

solids. As shown in Table 6, all three intrinsic equilibrium constants describing cadmium adsorption at the surface of Sigma anatase are greater than those of TiNano anatase. On the basis of these constants, our model estimates that the fraction of Cd^{2+} adsorption on Sigma anatase is 87% at pH 6, compared to 40% for TiNano anatase. This model prediction agrees well with our experimental data. Because the pH_{pzc} of the Sigma and TiNano anatase are similar (Figure 3), the smaller observed adsorption of Cd^{2+} on the nanometer-scale anatase might be due to intraparticle electrostatic effects, as noted previously. The different constant capacitance of Sigma Anatase (145 nm) versus TiNano anatase (40 nm) represents the differences in lateral repulsion of Cd on anatase particles of different sizes.[42]

Both Langmuir isotherm fitting and surface complexation modeling indicate that adsorption of Cd^{2+} on anatase nanoparticles is smaller than on large crystals and the adsorption is completely reversible. These results suggest that the adsorption mechanism of heavy metal adsorption on nanomter-scale anatase may be different from that of large crystals, and this will affect the transport of heavy metals in the environment. The differences in adsorption energy between nanometer-scale and large anatase may be related to intraparticle electrostatic effects or may be due to Ti-site disorder for nanocrystals with grain sizes of 20 nm or less.[20,63] Further research is under way to better identify the molecular origin of the size effect on heavy metal adsorption to nanoscale particles.

Acknowledgment. The financial support of the Center for Biological and Environmental Nanotechnology at Rice University and U.S. EPA Hazardous Substance Research Center/South & Southwest Region is greatly appreciated.

LA049334I

(63) Baurac, D.; Brown, E. Chemist, Material Scientists Have Big Questions About Tiny Particles. http://www.anl.gov/OPA/logos18−2/nanochem1.htm (accessed Feb 2003), Argonne National Laboratory, 2003.